Atmos. Chem. Phys. Discuss., 14, 18591–18640, 2014
www.atmos-chem-phys-discuss.net/14/18591/2014/
doi:10.5194/acpd-14-18591-2014

Atmospheric Chemistry and Physics Discussions

Tracing the second stage of Antarctic ozone hole recovery with a "big data" approach to multi-variate regressions

A. T. J. de Laat, R. J. van der A, and M. van Weele

Royal Netherlands Meteorological Institute, De Bilt, the Netherlands

Received: 28 May 2014 – Accepted: 30 June 2014 – Published: 14 July 2014

Correspondence to: A. T. J. de Laat (laatdej@knmi.nl)

Published by Copernicus Publications on behalf of the European Geosciences Union.

Abstract

This study presents a sensitivity analysis of multi-variate regressions of recent springtime Antarctic vortex ozone trends using a "big data" ensemble approach. Multi-variate regression methods are widely used for studying the variability and detection of ozone trends. Based on multi-variate regression analysis of total Antarctic springtime vortex ozone it has been suggested that the observed increase of ozone since the late 1990s is statistically significant and can be attributed to decreasing stratospheric halogens (Salby et al., 2011, 2012; Kuttippurath et al., 2013). We find that, when considering uncertainties that have not been addressed in these studies, this conclusion on ozone recovery is not warranted.

An ensemble of regressions is constructed based on the analysis of uncertainties in the applied ozone record as well as of uncertainties in the various applied regressors. The presented combination of ensemble members spans up the uncertainty range with about 35 million different regressions.

The poleward heat flux (Eliassen–Palm Flux) and the effective chlorine loading explain, respectively, most of the short-term and long-term variability in different Antarctic springtime total ozone records. The inclusion in the regression of stratospheric volcanic aerosols, solar variability, the Quasi-Biennial Oscillation and the Southern Annular Mode is shown to increase rather than to decrease the overall uncertainty in the attribution of Antarctic springtime ozone because of large uncertainties in their respective records.

Calculating the trend significance for the ozone record from the late 1990s onwards solely based on the fit of the effective chlorine loading should be avoided, as this does not take fit residuals into account and thereby results in too narrow uncertainty intervals. When taking fit residuals into account, we find that less than 30 % of the regressions in the full ensemble result in a statistically significant positive springtime ozone trend over Antarctica from the late 1990s to either 2010 or 2012. Analysis of choices and uncertainties in time series show that, depending on choices in time series and

parameters, the fraction of statistically significant trends in parts of the ensemble can range from negligible to more than 90 %. However, we were unable to detect a robust statistically significant positive trend in Antarctic springtime vortex ozone in the ensemble.

1 Introduction

An important question in 21st century ozone research is whether the ozone layer is starting to recover as a result of the measures taken to reduce emissions of Ozone Depleting Substances (ODS) as agreed on in the Montreal Protocol (UNEP, 2012) and subsequent amendments of the protocol.

The World Meteorological Organization has defined three different stages of ozone recovery (WMO, 2007). The first stage consists of a slowing of ozone depletion, identified as the occurrence of a statistically significant reduction in the rate of decline in ozone due to changing stratospheric halogens. The second stage revolves around the onset of ozone increase (turnaround), identified as *the occurrence of statistically significant increases in ozone – above a previous minimum value – that can be attributed to declining stratospheric halogens*. Note that what is meant by "statistically significant" is not specified. Finally, the third stage is the full recovery of ozone from ODSs, identified as when the ozone layer is no longer affected by ODSs, or alternatively, once stratospheric ozone levels have returned to pre-1980 values.

The first stage of ozone recovery has already been identified in observations to have occurred roughly in the late 1990s (WMO, 2007, 2011). The third stage is not expected to occur until somewhere halfway the 21st century or later (WMO, 2011). The spatial distribution of total ozone after the third stage probably differs somewhat from the pre-1980 distribution due to climate change – in particular changes in the stratospheric chemical composition and temperature structure (Bekki et al., 2011, and references therein).

As far as the second stage of ozone recovery is concerned, it has recently been argued that a statistically significant increase in ozone beyond a minimum and attributable to decreases in ODSs can be identified for the Antarctic ozone hole (Salby et al., 2011, 2012; Kuttippurath et al., 2013). To some extent this is surprising as it has long been thought that identification of the second stage of ozone recovery could only be expected after 2020 (e.g. Newman et al., 2006; Eyring et al., 2007). Those estimates were based on (model) simulations of ozone from which it is calculated when the ozone trend from a certain starting year onwards would qualify for "statistically significant", or in other words, would emerge from the year-to-year natural variations in ozone ("noise"). Such methods implicitly assume that ozone variations around the trend are not deterministic (random).

However, it has also long been established that many stratospheric ozone variations are in fact deterministic. Various processes have been identified that affect stratospheric ozone variability in the Southern Hemisphere on an inter-annual basis, like volcanic aerosols (Telford et al., 2009), the Southern Annular Mode (SAM) (Thompson and Wallace, 2000; Jiang et al., 2008), the poleward heat flux or Eliassen–Palm flux (EP flux) (Randel et al., 2002), solar variability (Soukharev and Hood, 2006), and the Quasi Biennial Oscillation (QBO) (Jiang et al., 2008). If the physics and chemistry are sufficiently understood, it might be possible to filter out part of the ozone variations from the ozone records, resulting in a smoother ozone record for which trend significance might be reached earlier. This approach, in essence, forms the basis of the suggested identification of the second stage of ozone recovery reported by Salby et al. (2011, 2012) and Kuttippurath et al. (2013).

However, none of these studies did systematically consider the uncertainties and potential errors in the proxies that were selected for the regressions. In addition, no motivation or discussion was provided for the choice of a specific ozone record, e.g. a consideration of taking annual, seasonal, and/or monthly means of total ozone and the integration over a chosen spatial domain.

Hence, we want to address the following question in this study: is the suggested detection of the second stage of ozone recovery robust when uncertainties in the regression parameters and for different selected ozone records are fully taken into account? This question is approached here with combined multiple scenario – Monte Carlo ensemble simulations using the same regression methodology as presented in Kuttippurath et al. (2013) but by inclusion of various uncertainties leading to a large ensemble of different regressions. We analyze this "big data" ensemble for robustness of the individual regressions.

Kuttippurath et al. (2013) considered different Antarctic vortex definitions and thus different vortex ozone records. They found that regression results were not very sensitive for the Antarctic vortex definition. Hence, we decided to use September–November Antarctic vortex core (poleward of 70° S) average total ozone column based on the Multi Sensor Reanalysis (MSR; van der A et al., 2010), also because from a practical point of view this definition does not require additional information about the location of the vortex edge. The selected regressors are the SAM, solar flux, QBO, EP flux, stratospheric volcanic aerosols and the Equivalent Effective Stratospheric Chlorine (EESC), similar as in Kuttippurath et al. (2013). The EESC can be used to estimate ozone trends. Kuttippurath et al. (2013) also calculated Piece Wise Linear Trends (PWLT) for estimating ozone trends as alternative for the EESC-based ozone trends, an approach we will follow here as well.

In this paper, we extend the analysis by introducing both several differing scenarios for the ozone record and regressor records of the EP flux, volcanic aerosols, and EESC. Monte Carlo variations were applied to the regressor records of the solar flux, QBO, SAM by adding random variations. While we focus on parameter uncertainties in this study, additional uncertainties do exist, for example with respect to possible time lags between regressors and the ozone record. The resulting ensemble of regression results provides a big data pool of about 35 million different regressions that is analyzed in terms of probability distributions of the explanatory power of the regressions, the ozone trends and corresponding uncertainties, and the regression coefficient values quantifying the dependence of ozone on a particular regressor. We also investigate if some way of optimization is possible for the chosen scenarios, and we discuss the likelihood of detection of the second stage of ozone recovery within the context of all uncertainties presented.

This paper is organized as follows. Section 2 describes the observational datasets used and the ozone and regressor scenarios or Monte Carlo simulations performed. Section 3 discusses the probability distributions of the explanatory power of the regressions, trends and regression values, including how the distributions depend on scenarios or Monte Carlo results. Section 4 discusses the question of detection of the second stage of ozone recovery, and in Sect. 5 everything is wrapped up and some conclusions are drawn.

2 Multivariate regression parameter uncertainties and errors

Online data sources of the ozone observation records and applied regressors can be found in the Supplement.

2.1 Method

A common method for analyzing total ozone records is the use of a multi-variate linear regression, a method that we will use in this paper as well. The goal of the method is to attribute both inter-annual as well as decadal variations in the ozone record to processes that are expected or known to affect the total ozone record (Kuttippurath et al., 2013, and references therein). In the regression, the total ozone variability (Y) as a function of time (t) is expressed as

$$
\begin{aligned}
Y(t) &= K && \text{(Constant)}\\
&+C_1\mathrm{HF}(t) && \text{(Poleward Heat Flux or Eliassen–Palm (EP) flux)}\\
&+C_2\mathrm{SAM}(t) && \text{(Southern Annual Mode index)}\\
&+C_3(\mathrm{SF}\times\mathrm{QBO})(t) && \text{(Solar Flux} \times \text{QBO index)}\\
&+C_4\mathrm{Aer}(t) && \text{(Stratospheric Aerosol optical depth)}\\
&+C_5\mathrm{Trend}(t) && \text{(Total ozone trend)}\\
&+\varepsilon(t) && \text{(Total ozone residual)}
\end{aligned}
$$

in which t is the time from 1979 to 2010 or 2012, K is a constant and regression coefficients C_1 to C_5 are the regression coefficients for the respective proxies. The ozone trend (C_5) can be related to the time-dependent equivalent effective stratospheric chlorine loading (EESC), a piece-wise linear trend before and after a pre-defined break year (PWLT) or two ordinary linear trends before and after a pre-defined break year (LINT). The PWLT and LINT regressions are calculated on the residual ozone after subtracting the fit of the first four regression variables from the ozone record, thereby implicitly assuming that the ozone residuals are only affected by changes in stratospheric halogens. For the PWLT regressions it is required that the linear regressions before and after the break year are continuous, i.e. these are connected at the break year. For the LINT regressions this is not required. The PWLT algorithm used here is described in Tomé and Miranda (2004).

The analysis of regression results will focus on two parameters that have previously been used in papers investigating Antarctic ozone recovery (Yang et al., 2008; Salby et al., 2011, 2012; Kuttippurath et al., 2013): the serial correlation between the regression-based "reconstructed" ozone record and the observations, and the post-break trends and trend significance. Since the focus of our paper is to investigate trend significance, not specifically what parameters can best explain Antarctic ozone, we will not look into detail at the usefulness of certain regressors. However, our analysis will provide indications of what are more and less useful regressors, which will be discussed.

In Sects. 2.2 to 2.9 the uncertainty in each of the proxies that is used as a regressor is discussed. These uncertainty ranges determine the spread in the ensemble that is used in the "big data" analysis. A summary of the regressor uncertainties and how they are incorporated in this study can be found in Table 1. The solar flux and QBO are combined into one proxy as discussed in Sect. 2.5.

2.2 Poleward heat flux (EP flux)

Figure 1 shows the poleward heat flux, here represented by the (vertical) EP flux (Andrews et al., 1987) at the 70 hPa level and averaged poleward of 40° S for the combined months of August and September, as well as the average EP flux available for a given year for a variety of datasets. Note that the datasets do not all completely overlap in time. Before 2000 there are considerable differences between the datasets. After 2000 these differences are smaller, which to some extent is traced to the lack of ERA40 data beyond 2001 and lack of JRA data beyond 2004. The lower panel shows the relative differences between the five datasets and their mean. The standard deviation of all data is 7.65 %, but from 2000 onwards only 2.67 %.

Another source of uncertainty in the use of the EP flux as proxy is the choice of the period for which the average EP flux is calculated. This choice depends on what is thought to be the relationship between variations in EP flux and ozone depletion. The basic theory states that the poleward movement of stratospheric air is proportional to the strength of the residual mean stratospheric circulation (Brewer–Dobson circulation), which in turn is driven by the poleward eddy heat flux. The poleward eddy heat flux is expressed by the upward component of the Eliassen–Palm flux that measures the upward transport of momentum by planetary waves (Andrews et al., 1987; Salby et al., 2012, and references therein). Planetary wave activity in the Northern Hemisphere affects Arctic Polar vortex stability and thus Arctic ozone depletion. However, to what extent this is similar in the Southern Hemisphere is still a topic of debate. The Arctic and Antarctic may behave either similarly (Weber et al., 2003, 2011) or not (Salby et al., 2012). This is because the notion of hemispheric similarities in how the EP flux

affects ozone depletion so far is heavily based on only one outlier year (2002 for the SH, 2011 for the NH).

Current research efforts try to gain a better understanding of the physical and photochemical mechanisms by which the heat flux and planetary wave action affects Antarctic stratospheric ozone. A recently proposed mechanism (de Laat and van Weele, 2011) involves a pre-conditioning of Antarctic inner stratospheric vortex air whereby stratospheric temperatures affect PSC formation which in turn affects the buildup of a halogen reservoir that later during Austral spring changes the rate of catalytic ozone destruction. This preconditioning mechanism explains some years with anomalous ozone depletion, but not all. For example, during Austral winter 2013 the Antarctic vortex remained largely undisturbed – opposite to 2010 and 2012, see de Laat and van Weele (2011) and Kleiciuck et al. (2011), thus allowing for widespread PSC formation and pre-conditioning the inner vortex air for efficient ozone depletion. However, from the start of Austral spring 2013 (halfway August) onwards the Antarctic stratospheric vortex got disturbed by planetary wave activity. As a result, the amount of springtime ozone depletion remained below what has been experienced during previous years with similar preconditioning. This suggests that there are multiple pathways as well as complicated interactions between chemistry and physics that can lead to reduced Antarctic springtime ozone depletion. Hence, it is unclear which regressor or regressors could act as proxies for these complex processes.

A further complicating factor is the disintegration of the Antarctic vortex, which is again controlled by planetary wave activity (Kramarova et al., 2014). The stability of the vortex determines how long the ozone depleted inner-vortex air remains intact after photochemical ozone depletion ceases during Austral spring. Variations in the duration of Antarctic vortex stability introduce variations in the Antarctic total ozone record which are not related to variations in photochemistry.

We attempt to reflect these issues in our uncertainty range for the proxy used to account for the EP flux variations in multivariate regressions. Salby et al. (2011, 2012) and Kuttippurath et al. (2013) use the August–September mean EP flux poleward of

40° S and at the 70 hPa level, the baseline also used in this study. Weber et al. (2011) uses the 100 hPa poleward heat flux rather than the 70 hPa heat flux and the average over the region between 45° S and 75° S rather than between 40° S and 90° S. They further show that there is no particular favorable wintertime month or period from the perspective of Antarctic springtime ozone depletion over which to average the EP flux. Hence there is a certain arbitrariness involved in selecting the optimum EP flux averaging period and region.

For our study we define eight different EP flux scenarios, using different periods, latitudes and heights (see Table 1), all based on the ECMWF ERA Interim dataset. Performing the same exercise as in Fig. 1 for these eight scenarios, the standard deviation of the EP flux time series is 21.5 %. This is considerably larger than the variability among the same EP fluxes of the different reanalysis datasets discussed above. Thus, the uncertainty in EP flux estimates largely originates in using different periods, latitudes and/or heights for which the EP flux is calculated, rather than in the use of different reanalysis datasets to calculate the same EP flux.

2.3 QBO

The Quasi-Biennial Oscillation (QBO) of the winds in the equatorial stratosphere has been discovered in the 1950s through the establishment of a global, regularly measuring radiosonde network (Graystone, 1959; Ebdon, 1960). The Free University of Berlin has compiled a long-term record from 1953 onwards of daily wind observations of selected stations near the equator. From these daily measurements monthly mean zonal components were calculated for pressure levels of 70, 50, 40, 30, 20, 15, and 10 hPa. For the period after 1979 only measurements from Singapore are used. The QBO data set is supposed to be representative of the equatorial belt since various studies have shown that longitudinal differences in the phase of the QBO are small. It should be noted, however, that some uncertainties arose at higher levels during the early years from the scarcity of observations. More information on the original data and their evaluation can be found in Naujokat (1986).

As proxy for the regressions we will use the 40 hPa QBO index, also used in Kuttippurath et al. (2013). Salby et al. (2011, 2012) chose to use 30 hPa winds instead. The relevancy of the choice of QBO index will be evaluated later. Information on the uncertainties in the monthly QBO data is not available. One indirect method to estimate the uncertainties is by examining QBO index variability close to the maximum and minimum of the QBO cycles, where the QBO index values remains more or less constant for some months. Assuming that during the maximum or minimum in the QBO phase variations from month to month are indicative of uncertainties in the QBO, we come up with estimated uncertainties of around 1.5–2.0 m s^{-1} in the zonal mean wind speeds.

2.4 Solar flux

Variations in incoming solar radiation – in particular the shorter ultraviolet wavelengths – have an effect on stratospheric ozone (e.g. Anet et al., 2013, and references therein). A standard proxy for variations in incoming solar radiation in ozone regression studies is to use the monthly mean 10.7 cm radio flux, as also used in Kuttippurath et al. (2013). This data set was obtained via NOAA/NESDIS/NGDC/STP.

However, there are other solar activity proxies available. Ideally, in absence of true UV spectral measurements, one would like to use a proxy that is representative for solar activity at those wavelengths where stratospheric ozone formation occurs, which is of roughly between 200 and 300 nm. Dudok de Wit et al. (2009) tried to identify the best proxy for solar UV irradiance, and concluded that proxies derived from a certain wavelength range best represent the irradiance variations in that wavelength band. Thus, the 10.7 cm radio flux might not fully represent solar UV variability. Using the results from Dudok de Wit et al. (2009) to analyze a set of seven solar activity proxies dating back to at least 1979 based on the solar2000 model and obtained from NOAA/NESDIS/NGDC/STP (F10.7, Lyman-alpha, E10.7, and the solar constant S), we will assume in our regressions that the uncertainty range associated with the solar proxy is approximately 15 % of the root-mean-square of the anomaly values.

2.5 The mixed solar-QBO index

In Kuttippurath et al. (2013) the effects of solar variability and QBO variability are combined into one proxy. Solar effects on winter polar Antarctic stratospheric temperatures depend on the phase of the QBO (Labitzke, 2004). If the QBO is westerly (easterly), the temperatures vary in phase (out of phase) with solar activity. It has been proposed by Haigh and Roscoe (2006) and Roscoe and Haigh (2007) to combine the QBO and solar activity into a new regression index that takes this effect into account:

$$\text{Solar–QBO index} = (\text{Solar} - S_\text{m}) \times (\text{QBO} - Q_\text{m})$$

In which S_m is the mean of the solar flux and Q_m the mid point of the QBO range. However, as Roscoe and Haigh (2007) note, this new index is rather sensitive to the choice of S_m and Q_m, in particular as the index is by construction the product of two anomaly fields, and thus sensitive to sign changes. In addition, the choice of S_m and Q_m is also arbitrary. Roscoe and Haigh (2007) solve this by selecting the means for which the best total ozone column regression results are obtained. However, the best regression results may not necessarily mean that the regressor is the best representation of the underlying physical mechanism, in particular as regression results also depend on other proxies and in principle there can be a cancellation of errors from different proxies in the regression. Thus, the sensitivity of the combined solar-QBO index on the calculation method of the anomalies must be further investigated.

Figure 2 shows the resulting solar flux–QBO index time series, given various assumptions in its calculation. Clearly there is a considerable variability in the index values. The lower plot shows that the variability for every single anomaly varies by ±200 %. This is rather large compared to the estimated uncertainties in both individual solar flux and QBO proxies. Hence, using a combined solar flux–QBO proxy introduces a considerable amount of additional uncertainty. For the uncertainty range in our regressions we construct 100 Monte Carlo time series in which for each single solar-flux QBO index value random Gaussian noise is added with an amplitude of 200 % of the index value.

2.6 Southern Annular Mode

The Southern Annular Mode (SAM) is a widely used index that reflects the zonal symmetry of the tropospheric circulation in the Southern Hemisphere. The symmetry of the Southern Hemisphere circulation has long been identified as an important mode of variability of the Southern Hemisphere climate. A positive index is characterized by anomalously high surface pressure at mid-latitudes and anomalously low surface pressure at latitudes closer to Antarctica.

The SAM used in this study is derived from NOAA. It is based on Empirical Orthogonal Functions (EOF) applied to the monthly mean NCEP/NCAR reanalysis 700 hPa height anomalies poleward of 20° S for the Southern Hemisphere, with the seasonal cycle being removed. The monthly SAM index is constructed by projecting the daily and monthly mean 700 hPa height anomalies onto the leading EOF mode. Both time series are normalized by the standard deviation of the monthly index (1979–2000 base period). Since the leading pattern of SAM is obtained using the monthly mean height anomaly dataset, the index corresponding to each loading pattern becomes one when it is normalized by the standard deviation of the monthly index.

However, there is no unique SAM index due to the existence of different meteorological datasets and different methods to quantify the symmetry of the Southern Hemisphere circulation. Kuttippurath et al. (2013) use the AntArctic Oscillation (AAO) index, which is in fact a certain choice of SAM index. A study by Ho et al. (2012) provides a comprehensive analysis of eight different SAM indices. Their analysis shows that the correlation (R^2) between the indices varies between 0.45 and 0.96 for seasonal values and 0.73 and 0.96 for monthly values. This corresponds with random (Gaussian) variations between 20–100 % (root-mean-square value). For most of the indices the correlation is better than 0.75. As a point of reference, adding random Gaussian noise of 50 % to a time series of a parameter and calculating its correlation with the original time series results to a correlation (R^2) of almost 0.8.

For the uncertainty analysis we construct 100 Monte Carlo time series in which for each single SAM index value Gaussian noise is added with – to be on the conservative side – an amplitude of 100 % of the index value.

2.7 EESC loading

Uncertainties in the estimates of the EESC loading originate from two factors: the mean age-of-air, which reflects how fast stratospheric halogen concentrations decline due to transport velocity of halogen poor tropospheric air from the tropical stratosphere to the polar stratosphere, and the so-called "fractional release", the rate with which Ozone Depleting Substances (ODSs) release chlorine and bromine in the stratosphere. ODSs typically have not yet been dissociated when they enter the stratosphere at the tropical tropopause, and thus have fractional release values of zero. After transiting through the upper stratosphere, the ODSs in an air parcel get fully dissociated due to their exposure to energetic radiation and the fractional release values get close to 1.0 (Newman et al., 2007).

To complicate matters, the mean age-of-air in the stratosphere is not a constant but varies with latitude, height and season (Stiller et al., 2008). On average, the age-of-air increases with height, i.e. it takes longer for tropospheric air to travel higher in the stratosphere, and the age-of-air also increases towards the poles because of the time it takes for air to travel from the tropical "source" region to higher latitudes. In the Antarctic vortex regions there is a strong seasonal dependence of the age-of-air due to the isolation of inner vortex air during Austral winter and spring, while upper stratospheric and mesospheric air slowly descends in the Antarctic vortex. The descending air is particularly "old" air and causes strong age-of-air gradients in the wintertime polar vortex. Stiller et al. (2008; their Fig. 7) show that the age-of-air almost triples going up from 15 km (θ = 400 K; age-of-air ~ 4 years), to 20 km (θ = 400 K; age-of-air ~ 7 years), to 25 km (θ = 600 K; age-of-air ~ 9 years), to finally 30 km (θ = 750 K; age-of-air ~ 11 years). How to account for this variability in a regression is unclear, but it is unlikely that one age-of-air value can be attributed to the total ozone column.

Moreover, ozone variability in the Antarctic vortex is determined by different processes at different altitudes. Halogen related ozone depletion typically maximizes between 15–20 km altitude (∼ 100–50 hPa, US Standard atmosphere 1976; θ = 400–500 K), whereas the effect of vortex stability on ozone depletion is seen predominantly between 20–30 km altitude (∼ 50–10 hPa; θ = 500–750 K) (de Laat and van Weele, 2011). Thus, total ozone columns observations which are vertically integrated amounts of ozone are being affected by different processes at different altitudes.

The age-of-air may also not be constant over the time period over which ozone trends are determined. Due to a changing climate the stratospheric circulation may speed up (e.g. Engel et al., 2009; Bunzel and Schmidt, 2013), causing a decrease in the age-of-air with increased warming, which obviously then depends on the exact warming. This introduces yet another uncertainty for the periods from 1979 to 2010 or 2012 that are considered in this study.

The age-of-air uncertainties do not manifest themselves as a random process, which would make it useful for applying a Monte Carlo method, but as a structural uncertainty, i.e. the entire EESC shape would change for different parameter settings. Such uncertainty could be captured by applying a parametric bootstrap rather than a Monte Carlo approach. However, such parametric approach would also not suffice because we use total column observations and we know that ozone at different altitudes would be affected by different parameter values.

A pragmatic approach with regard to the sensitivity of the regression to EESC values is testing the robustness of the regression results as a function of the assumed EESC time evolution. For the uncertainty analysis we assume three different EESC scenarios with an age-of-air of 2.5, 4 and 5.5 years and a half-width of, respectively, 1.25, 2 and 2.75 years. Largest differences between the three scenarios are in their post-peak trend in EESC (see later on in Fig. 3).

2.8 Volcanic aerosol

Aerosols from sufficiently strong volcanic eruptions can reach the stratosphere and affect stratospheric ozone chemistry. In particular strong eruptions occurring in the tropics can have long lasting effects on stratospheric ozone. Aerosols reaching the tropical stratosphere are slowly transported towards middle and high latitudes. It can take up to a decade before the stratosphere is cleared. Volcanic eruptions at middle and high latitudes have much shorter lasting effects. These aerosols enter in the descending branch of the stratospheric circulation and will be relatively quickly removed from the stratosphere.

The short-term effect of stratospheric volcanic aerosols is heating of the stratospheric layer which affects stratospheric ozone in the tropical belt. The dominant long-term effect of stratospheric volcanic aerosols on global and polar ozone is however the increase in aerosol surface area density and subsequent heterogeneous ozone loss. Model simulations of volcanic aerosol effects on stratospheric ozone suggest that in particular under cold conditions (high latitude, wintertime, lower stratosphere) total ozone columns can be reduced by up to 10–15 % (Rozanov et al., 2002). During other seasons, total ozone column depletion by volcanic aerosols is of the order of a few percent.

Since 1979 two major tropical volcanic eruptions have affected stratospheric ozone: El Chichón, Mexico, in 1982, and Pinatubo, Philippines, in 1991. Although the total amount of stratospheric aerosols by both eruptions has been characterized relatively well, there appear to be considerable uncertainties associated with the time evolution of the aerosol amounts in the Southern Hemisphere. A brief and incomplete survey of a latitudinal volcanic aerosol radiative forcing data (Ammann et al., 2003) and a global volcanic aerosol proxy record (Crowley and Unterman, 2013) as well as the standard volcanic aerosol index used in Kuttippurath et al. (2013) – aerosol optical depth, Sato et al. (1993) and updates, available via NASA GISS – all show that there are large differences between the El Chichón aerosol peak relative to the Pinatubo peak. Large differ-

ences are seen in global, hemispheric and Southern Hemisphere (Antarctic) aerosol amounts as well as differences in the exact timing of the peak aerosols (Sato et al., 1993; Ammann et al., 2003; Crowley and Unterman, 2013). The El Chichón aerosol peak relative to the Pinatubo peak for high Antarctic latitudes can be similar (Ammann et al., 2003), about three times smaller (Sato et al., 1993) to (globally) eight times smaller (Crowley and Unterman, 2013). The Pinatubo peak aerosol in the Southern Hemisphere was about half the size of the global-mean Pinatubo peak (Ammann et al., 2003).

Kuttippurath et al. (2013) shift the Southern Hemisphere aerosol data by six months to account for the transport of aerosols. Although they report that the six month shift results in the best statistics, the analysis presented in the previous section shows that the effect of the shift is relevant for the shape of the volcanic aerosol changes, but does not introduce variations as large as the other variations in volcanic aerosol indices. Given that a time shift is included in the 6 scenarios defined above, we do not add additional time shifts in the aerosol record.

We define six volcanic aerosol scenarios that reflect the uncertainty in the volcanic stratospheric aerosol records. Base scenario is the scenario used in Kuttippurath et al. (2013) which in turn uses the NASA GISS stratospheric aerosol record. A second scenario is with the Pinatubo aerosol peak comparable to El Chichón aerosol peak, the Pinatubo peak twice the El Chichón peak, and the Pinatubo peak five times the El Chichón peak. The uncertainty in timing of the Southern Hemispheric aerosol peak is considered by a shift of the El Chichón peak one year back compared to the Pinatubo peak and a shift of the Pinatubo peak one year back compared to El Chichón peak.

2.9 Ozone scenarios

It is a priori unclear what would be the most appropriate ozone scenario to use in the regression. Both Salby et al. (2011, 2012) and Kuttippurath et al. (2013) use the September–November three-month averaged total ozone record. However, as discussed in the introduction, different processes affect ozone during different periods.

Studies in the literature use very different periods for averaging ozone to investigate Antarctic ozone trends. We define eight different ozone scenarios to reflect the ozone records used in literature (see also de Laat and van Weele, 2011). Apart from the September–November three-month averaged total ozone record we also use averages of total ozone over the month of September, the month of October, the two-month period September–October, a very long period (19 July–1 December), a very short 10 day period (21–30 September), the period 7 September–13 October, and a year-dependent "worst" 30 day period (30 day average with the largest Ozone Mass Deficit).

2.10 Other uncertainties

Kuttippurath et al. (2013) address two other important uncertainties for the determination of the ozone trend. First, the area over which the ozone record is defined (Inside Vortex, Equivalent Latitude 65–90° S, and Vortex Core). The area is important for the absolute amounts of ozone depletion but Kuttippurath et al. (2013) show it is much less for the differences in trend. That is, the uncertainties in the estimated linear trend dominate the uncertainties due to different areas over which the ozone anomalies are calculated. A second uncertainty on their ozone trend derives from the use of different ozone datasets (ground-based, TOMS/OMI and MSR). Also here the uncertainties in the estimated linear trend dominate the uncertainties due to the different data sets. Hence, we do not include these uncertainties in our analysis.

In addition, there are many studies trying to identify the moment where ODSs stop increasing and/or where ozone stops decreasing. The maximum ODSs appears somewhere between 1997 and 2000 (Newman et al., 2007), depending on geographical location and height. However, due to saturation effects – there are more than sufficient ODS present to destroy all Antarctic ozone – the moment where ozone starts to be affected by decreasing ODSs may actually be later (Kuttippurath et al., 2013; Kramarova et al., 2014).

The moment of a structural break in ozone based on observations indicates an early break around 1997 (Newchuch et al., 2003; Yang et al., 2008). However, some pro-

cesses affecting stratospheric ozone vary on long time scales – solar effects and volcanic eruptions come to mind – which may affect the observations-based analysis of break points (Dameris et al., 2006). Note that we confirm this break year of 1997 based on a applying a break-point analysis algorithm to the MSR ozone record (not shown). Hence, we decided to use three different break years that have been identified and/or are most commonly used: 1997, 1998 and 1999.

2.11 Selected uncertainties ranges and ozone record scenarios

Figure 3 shows the baseline regressor time series and the scenarios for ozone, the EP flux, EESC loading and volcanic aerosols. A total of 100 different solar flux–QBO index and SAM index time series is used to span their uncertainty range (not shown in Fig. 3). All scenarios and Monte Carlo results combined provide 11.5 million different choices for the regressions ($100 \times 100 \times 8 \times 8 \times 6 \times 3$). Ozone trends are calculated based on the EESC loading, using a piecewise linear trend (PWLT) analysis as well as using a regular linear trend (LINT) pre and post a given break year. For the PWLT and the LINT ensembles the three different EESC scenarios are irrelevant. Instead, the sensitivity of the regressions is tested using three different break years (1997, 1998 and 1999). In total we analyze approximately 34.5 million different trends using the EESC, PWLT and LINT scenarios.

Note that by basing our analysis on both different ozone and EP flux scenarios certain time-lag relations are taken into account. It should also be noted that the use of such a wide range of scenarios indicates that much remains unclear about what best describes Antarctic ozone depletion and the time-lag relations between ozone and explanatory variables.

3 Scenario analysis

3.1 Reproducing Kuttippurath et al. (2013)

First a multi-variate regression is performed similar to Kuttippurath et al. (2013) in which the MSR dataset is used within the Vortex core (70–90° S). The results are summarized in their Fig. 5 and Table 4 which are duplicated here in Table 2 along with the results from our basic regression.

Our results reproduce the results from Kuttippurath et al. (2013), although there are minor differences in the absolute numbers, most likely related to differences in EP fluxes (J. Kuttippurath, personal communication, 2013). The trends for the periods 1979–1999 and for 2000–2010 are of comparable magnitude in both studies, as well as the PWLT significance levels for the period 1979–1999 and the EESC trends for both 1979–1999 and 2000–2010. The magnitude of the recovery for 2000–2010 based on the PWLT is a bit larger but the trend is not statistically significant (neither are our LINT trends nor our PWLT and LINT trends for 2000–2012). Note that the LINT trends differ from the PWLT trends, in particular for the post 2000 period. The comparison between PWLT vs. LINT results will be discussed later in the context of sensitivities to regressor uncertainty. For the correlation of the regression model with the ozone record we obtain a value of 0.86 (R^2) comparable to the 0.90 (R^2) reported in Kuttippurath et al. (2013). Thus, the results are sufficiently similar to proceed with studying the effects of the uncertainties in regressors and ozone record scenarios on the regression results.

3.2 Ozone record and regressor correlations

Before analyzing the ensemble of regression results it is important to investigate the correlations between the different regressors. If correlations between regressors are too large, they cannot be considered to be independent, and it should be decided which one to omit from the analysis, as the regression otherwise cannot separate which

variability is related to which regressor. Furthermore, it is a priori useful to understand how regressors correlate with the ozone record, as a small correlation implies that a regressor can only explain a limited amount of ozone variability.

Table 3 shows the mean correlation between the different regressors and their 2σ spread based on the ozone record and regressor selections and/or Monte Carlo results (SAM, SF × QBO index). The EP flux correlates positively with the EESC and negatively with the SAM and, to a lesser extent, also with the SF × QBO index. The other regressors do not show significant cross-correlations. Only for a few individual ozone record scenarios, regressor selections and Monte Carlo results cross-correlations are found to exceed 0.5.

The uncertainty in the correlations with the ozone records ranges between about 10 % and 20 % for each of the regressors. Small cross-correlations between the regressors however do not provide a justification for a priori omitting one of the regressors.

3.3 Trends

Figure 4 shows the probability distributions of the ozone trends for 1979-BREAK and BREAK-2012 periods, in which BREAK is the break year which can either be 1997, 1998 or 1999. For the 1979-BREAK period the distribution of EESC and LINT trends are comparable, while the PWLT ozone trends are considerably larger. However, for the BREAK-2012 trends the probability distributions are very different. The EESC trends show a tri-modal distribution which is absent in the PWLT and LINT trend distributions. The tri-modal distribution reflects the three different post-1997 EESC trends (see also Fig. 3). Furthermore, similar to the 1979-BREAK trends, the PWLT trends are larger than the LINT trends. The need for the PWLT to connect at the break point results in larger trends than would be the case for linear trends for each period separately. The PWLT cannot capture the smooth transition of halogens from increasing to decreasing before and after BREAK. In addition, the tri-modal EESC trend probability distribution for BREAK-2012 shows that in the linear regression the EESC fit is determined by the 1979-BREAK period more than by the BREAK-2012 period. This is not surprising

because the trends for the 1979-BREAK period are larger and cover a longer period than for BREAK-2012.

Figure 4 shows the probability distribution of the regression model correlations with the ozone record for all regressor combinations. The EESC-based correlations are larger than the PWLT and LINT correlations, while the LINT correlations are slightly larger than the PWLT correlations. Hence, the EESC trend model appears to be the better fit model for Antarctic ozone trend variations over the 1979–2012 time period than the PWLT and LINT model, a finding consistent with Knibbe et al. (2014).

In passing we note that the auto-correlation of the ozone residuals is small, indicating that the auto-correlation present in the ozone record (e.g. Fioletov and Shepherd, 2003; Vyushin et al., 2007) is related to some of the processes described by the regression parameters and can be removed by the multi-variate regression. Auto-correlation thus does not have to be taken into account in the trend significance calculation.

3.4 Regression model performance: sensitivity to EP flux and ozone record scenarios

Sensitivities of the PWLT-based and EESC-based regressions to the ozone and EP flux scenarios are shown in Fig. 5. PWLT-based regressions show no preference for a particular ozone record scenario (Fig. 5a). The September-October-November, September–October, September or "worst" 30 day ozone record scenarios all lead to similar distributions. For the EESC-based regressions the "worst" 30 day ozone scenario outperforms the other scenarios (Fig. 5b), while the September–October ozone record scenario is found to give closest correspondence. There is no clear dependence of regression model performance on the EESC age-of-air scenario (see Supplement Fig. S1).

PWLT regressions with EP fluxes for the period July–September and September-only lead to better regression results (Fig. 5c), whereas for the EESC regressions the July–September EP flux performs slightly better than the 100 hPa scenario, 45–75° S scenario and the August–September scenario (Fig. 5d). The distributions for the LINT

model are similar to the PWLT distributions (see Supplement Fig. S2). Both PWLT and LINT regressions show a slightly better performance when using 1997 as break year instead of 1998 and 1999 (not shown), consistent with studies of trend-break analyses of ozone indicating that 1997 is the most likely break year in the ozone record, (Chehade et al., 2013).

3.5 Regression coefficient value sensitivity

Volcanic aerosols have little impact on the explanatory power of the regression results, as already indicated by lack of correlation of this regressor wih the ozone record. The PWLT regression coefficient values show that the effect of volcanic aerosols on ozone can be either positive or negative (see Fig. 6), largely depending on the amount of the Pinatubo aerosols relative to El Chichón aerosols. The EESC regressions show a similar sign dependence of ozone on volcanic aerosol. None of other parameters (EPFLUX scenario, Ozone scenario) have a sign-dependent effect on the aerosol regression coefficient value for both the EESC and PWLT scenarios. The strong sensitivity of the volcanic aerosol regression value – including sign changes – to either aerosol or EESC scenario indicates that volcanic aerosols should be excluded from the multivariate regression altogether, because there is insufficient information in the Antarctic ozone record to constrain the ozone – volcanic aerosol relation.

For the solar flux–QBO index (Fig. 7a) we find no clear dependence of regression coefficient values on any of the scenarios or parameters. The probability distributions are Gaussian-shaped, with the PWLT distribution being slightly broader and slightly skewed to negative regression coefficient values but with a longer tail to positive regression coefficient values.

The SAM regression coefficient values also show a continuous random distribution while the overall dependence is negative (Fig. 7b). A positive phase of the SAM leads to more ozone depletion than a negative phase of the SAM. This is a well known two-way effect: tropospheric circulation changes affect Antarctic stratospheric ozone on the short term, while the long term changes in Antarctic ozone have affected the

tropospheric circulation in the Southern Hemisphere (Kirtman et al., 2013; IPCC AR5, Ch. 11, Sect. 11.3.2.4.2 and references therein). The probability distribution of the EESC regression coefficient values is skewed towards less negative SAM regression coefficient values, related to a consistent signal in EPFLUX scenario dependence (see Table 3).

For the EPFLUX the regressions generally show a positive dependence (Fig. 7c), with larger EESC-based regression coefficient values than PWLT-based regression coefficient values. Some PWLT-based regressions result in a negative regression coefficient value, particularly for the August-only EP flux scenario.

3.6 Optimal regressor and ozone record scenarios

Based on the analysis of the entire ensemble presented here it might be possible to chose an optimal set of regressors as well as an optimal ozone record scenario for Antarctic ozone trend analysis. Best explanatory power is obtained using the EESC as estimator for the long-term ozone trends with an age-of-air of 4 years (half width of 2 years). The optimal ozone record to analyze the second stage of ozone recovery turns out to be the “worst 30 day”, which is the 30 day period with the largest ozone mass deficit. Best correlations are found for the average July–September EP flux as regressor. For the PWLT- and LINT-based regressions these findings are the same. Alternatively, the September-October-November, September–October or 7 September–30 October ozone record scenarios might also suffice, while the September-only EP flux could be used instead of the July–September EP flux.

The optimal break year for both the PWLT- and LINT-based regressions is 1997, which corresponds with the peak chlorine content in the stratosphere and thus the first stage of ozone recovery. For all regression models volcanic aerosols do not seem to be a useful regressor for springtime Antarctic ozone records, given that even the sign of their effect on ozone is unclear for the Antarctic ozone hole.

Figure 8 illustrates what the best single regressions in the entire ensemble for all three regression models separately look like. The best EESC-regression correlation

(R^2 = 0.95) was found for a case with September-October-November ozone, July–September EP flux and an EESC with an age-of-air of 4 years. For the best LINT-regression correlation (R^2 = 0.90) and best PWLT-regression correlation (R^2 = 0.88) these were the same with again 1997 as optimal break year. Reason for the high explanatory power is that in all three cases the SAM anomalies align with strong ozone peaks whereas the solar flux–QBO index random variations align with the smaller ozone anomalies.

4 Discussion: second stage of ozone recovery and trend significance

Given the broad range of outcomes for the different types of regressions and regressors, an important question is not only if ozone has started to increase after the late 1990s, but also if the trend is statistically significant and can be attributed to declining stratospheric halogens, which is required by WMO for the second stage of ozone recovery to be formally identified. The EESC-based regressions all show significant trends but the post-BREAK EESC change is so gradual that non-significance of trends in ozone attributed to changes in EESC is de facto impossible. However, this gradual decrease in EESC does not reflect the residual unexplained ozone variations, which presumably is the "noise" from which the signal is expected to occur. In addition, the ensemble only includes three EESC scenarios, which yield a wide range of post-break ozone trends. As discussed in Sect. 2, it is a priori not clear which EESC scenario is the optimal one or if it is even appropriate to use just one EESC scenario. Hence, a regression of EESC-based ozone recovery results in ozone trend confidence intervals that do not represent the actual uncertainties related to the EESC scenario and the ozone record. It is therefore more relevant to investigate if the other post-BREAK trends – PWLT or LINT – are statistically significant as they use the ozone fit residuals for their significance calculation.

Figure 9 shows the probability distribution of correlations (R^2) of the PWLT regression models vs. ozone for the entire Monte Carlo dataset, as well as the fraction of

post-break PWLT trend estimates that are statistically significant (2σ) for both the periods ending in 2010 and 2012. Results indicate that trends only become statistically significant beyond a certain explanatory power of the regression model. This is not surprising: only when ozone residuals after removing the regression results are sufficiently small can the post-break trend become statistically significant. This automatically requires a high correlation between the ozone record and the selected regression model. The analysis here shows that statistically significant trends require a correlation (R^2) of at least approximately 0.70. Furthermore, only for high ozone-regression model correlations ($R^2 > 0.85$) the majority of trends become statistically significant. In addition, Table 4 shows that the number of significant trends depends on the exact break year, with only 0.9 % of the 2000–2010 PWLT trends being significant and 21.5 % of the 1998–2012 PWLT trends. For regressions ending in 2010 the percentage statistically significant trends is smaller than for regressions ending in 2012. This is not surprising as the regression trend error decreases with increasing number of points for which the trends are calculated (see the Supplement Eq. S2).

In Sect. 3.6 the results of the ensemble were analyzed to determine optimal scenarios in terms of explanatory power (R^2). However, the second stage of ozone recovery requires also a statistically significant post-break year trend. We therefore analyzed the percentage of statistically significant post-break trends in the ensemble for the PWLT-based regressions. We focus on the ozone record and EP flux scenarios as the uncertainties associated with these two parameters are the most important ones, as discussed before. Table 5 shows the percentage of regressions for each combination of ozone record and EP flux scenarios that is statistically significant. There are large differences in the fraction of statistically significant PWLT-based trends, ranging from less than 0.1 % (multiple combinations) to over 50 % (October ozone, September EP flux). Furthermore, the ozone scenario resulting in the largest fraction of statistically significant trends (October ozone) was not found to be the month resulting in the largest explanatory power of the regressions. In addition, there are multiple EP flux scenarios resulting in a large fraction of statistically significant trends, whereas analy-

sis of explanatory power results suggest that the July–September and September EP flux scenarios result in the best explanatory power. Similarly, there are more ozone scenarios that qualified for the largest explanatory power results than scenarios with the largest fraction of statistically significant trends (September–October and October). In particular, the "worst 30 day" ozone scenario results in high explanatory power but provides only a small fraction of statistically significant trends.

Table 6 shows the same results as Table 5, but only for the break year 1997 and the period ending in 2012. Although the scenario combinations resulting in small or large fractions of statistically significant trends are similar to those in Table 5, the fractions are much higher. This is consistent with the earlier notion that 1997 is probably the best break year. In particular, for the October ozone scenario the fractions of statistically significant trends approach the 95 % level for various EP flux scenarios.

It is tempting to interpret these results as being close to the required significance for identification of the second stage of ozone recovery. However, by comparison the trend significance with an analysis in terms of largest explanatory power the results are much less convincing. Given that it is currently unclear what constitutes the best scenarios, detection of the 2nd stage of ozone recovery based on just one arbitrary selected regressor – ozone record combination does not reflect the structural uncertainties present in the underlying data.

Despite using fewer regressors, Salby et al. (2011, 2012) find much higher explanatory power of their regressions (R^2 = 0.98) then found here and before by Kuttippurath et al. (2013) (R^2 = 0.90 or less). Our attempts to reproduce the results by Salby et al. (2011, 2012) following the same 2-parameter regression were unsuccessful. We found an explanatory power (R^2) of approximately 0.7 only, which is consistent with the findings presented in this paper. It is unclear what causes the difference. It is also unclear how Salby et al. (2011, 2012) exactly derive their ozone record (P. Newman, NASA, personal communication, 2012). Unfortunately, none of the authors of the Salby et al. (2011, 2012) papers are at the moment active in this field of research, which hampers resolving this issue. Nevertheless, given the range of results of our sensitivity

analysis we are confident that the trend significance of the Salby et al. (2011, 2012) results would have turned out insignificant if the uncertainties in their regression model had been taken fully into account.

5 Conclusions

The primary goal of this study was to investigate whether or not the 2nd stage of ozone recovery – a statistical increase in ozone attributable to ozone depleting substances – can be detected, given structural uncertainties in underlying data. A detailed sensitivity analysis of widely used multi-variate regression analysis of total ozone columns was presented focusing on Antarctic springtime ozone. By combining regressor scenarios and Monte Carlo simulations for various ozone record scenarios, a total of approximately 34.5 million different multivariate regressions were performed.

Use of the post-BREAK trends based on fitting the EESC to the total ozone record should be avoided, as these trends are solely based on the pre-defined EESC shape and the EESC-fit based trend uncertainties do not take the ozone fit residuals into account. When considering the ozone fit residuals in the trend errors, we argue that it cannot be concluded that the second stage of ozone recovery has arrived, as there is no obvious argumentation which of the many possible scenarios and scenario combinations to prefer. Although it is possible – within the uncertainties defined in this study – to derive at statistically significant increases in ozone since the late 1990s, for only a minority of regressions (from nearly 0 % to 30 % at maximum) a statistically significant increase is determined. Note that our results for ozone trends are nevertheless consistent with the second stage of recovery – we do find increases ozone since the late 1990s that can be attributed to decreases in ODS for selected combinations of regressors.

Our analysis reveals typical caveats and pitfalls of multivariate regressions. For example, the higher the explanatory power of the regression model, the more likely it is that a statistically significant increase in ozone is detected. Furthermore, there are sce-

nario combinations for which most regressions result in statistically significant trends (one example almost reaching 95 %). It is therefore tempting to declare these scenarios as "the best" representations of for example ozone and EP fluxes. However, there do not appear to be physically compelling arguments why to prefer this scenario combination over other combinations. We conclude that care has to be taken with the results of multi-variate regression analyses of Antarctic ozone.

Most of the Antarctic total ozone record can be explained by the EP flux, the SAM, and slowly decreasing and increasing ozone before and after the late 1990s, either described by linear trends or by the EESC. However, we find that the use of EESC to describe how Antarctic ozone changes as a result of changing stratospheric halogen concentrations is problematic. The EESC scenario results in overconfident ozone trend uncertainties as it does not consider the ozone residuals in calculating the trend uncertainties nor does one particular scenario reflect that the ozone trends are highly sensitive to the chosen scenario.

There appears little justification in including volcanic aerosols, the solar-flux and QBO in the analysis of trends in Antarctic springtime ozone depletion. For the volcanic aerosols there is only very limited time information present in the ozone record (essentially two isolated peaks). A similar conclusion was reached by Knibbe et al. (2014), who found little evidence for volcanic effects on total ozone throughout the Southern Hemisphere. Furthermore, Poberaj et al. (2011) also reported little impact of volcanic aerosols from the Pinatubo eruption on Southern Hemispheric ozone, attributing it to dynamical conditions favoring more poleward transport of ozone from the tropics and mid-latitudes than usual, thereby "*overcompensating the chemical ozone loss . . . and reduce the overall strength of the volcanic ozone signal*".

The lack of correlation between Antarctic ozone and the solar-flux and QBO may appear at first sight rather surprising, as it is a well known and well documented phenomenon at least outside of the polar regions. However, Knibbe et al. (2014) also did not find a significant impact of either the solar flux or QBO on Antarctic (and Arctic) ozone trends, while there are clear and significant solar flux and QBO signals in the

total ozone column records. Part of the explanation might be in the isolation of the springtime vortex from the rest of the stratosphere.

Finally, we found indications that increasing the record length also increases the number of statistically significant trend estimates. Hence, it can be anticipated that it is only a matter of time until the majority of scenarios investigated in this study will show a statistically significant increase in Antarctic ozone. As outlined in the introduction, previous studies have indicated that without filtering the ozone record for non-ODS influences the second stage of recovery the Antarctic ozone-hole is not expected until approximately 2020 or later. It still remains possible that – using a multi-variate regression method to remove non-ODS influences from the total ozone record – recovery of the Antarctic ozone-hole will be detected before 2020. Future updates of the analysis in this paper by extending the ozone record should provide indications whether this moment approaches fast or not.

Acknowledgements. The authors wish to thank the following authors of chapter 3 of the 2014 WMO ozone assessment report – Sophie Godin Beekmann, Martin Dameris, Peter Braesicke, Martin Chipperfield, Markus Rex and Michelle Santee – as well as John Pyle, Ted Shephard and in particular Paul Newman for encouraging us to write this paper.

References

Ammann, G., Meehl, A., Washington, W. M., and Zender, C. S.: A monthly and latitudinally varying volcanic forcing dataset in simulations of 20th century climate, Geophys. Res. Lett., 30, 1657, doi:10.1029/2003GL016875, 2003.

Andrews, D. G., Holton, J. R., and Leovy, C. B.: Middle Atmosphere Dynamics, Academic Press, Orlando, Florida, 489 pp., 1987.

Anet, J. G., Rozanov, E. V., Muthers, S., Peter, T., Brönnimann, S., Arfeuille, F., Beer, J., Shapiro, A. I., Raible, C. C., Steinhilber, F., Schmutz, W. K.: Impact of a potential 21st century "grand solar minimum" on surface temperatures and stratospheric ozone, Geophys. Res. Lett., 40, 4420–4425, doi:10.1002/grl.50806, 2013.

Bekki, S., Bodeker, G. E. (Coordinating Lead Authors), Bais, A. F., Butchart, N., Eyring, V., Fahey, D. W., Kinnison, D. E., Langematz, U., Mayer, B., Portmann, R. W., Rozanov, E., Braesicke, P., Charlton-Perez, A. J., Chubarova, N. E., Cionni, I., Diaz, S. B., Gillett, N. P., Giorgetta, M. A., Komala, N., Lefévre, F., McLandress, C., Perlwitz, J., Peter, T., and Shibata, K.: Future ozone and its impact on surface UV, in: Scientific Assessment of Ozone Depletion: 2010, Global Ozone Research and Monitoring Project, chap. 3, Report No. 52, 1–516, Geneva, Switzerland, 2011.

Bunzel, F. and Schmidt, H.: The Brewer–Dobson Circulation in a Changing Climate: impact of the Model Configuration, J. Atmos. Sci., 70, 1437–1455, doi:10.1175/JAS-D-12-0215.1, 2013.

Chehade, W., Burrows, J. P., and Weber, M.: Total ozone trends and variability during 1979–2012 from merged datasets of various satellites, Atmos. Chem. Phys. Discuss., 13, 30407–30452, doi:10.5194/acpd-13-30407-2013, 2013.

Crowley, T. J. and Unterman, M. B.: Technical details concerning development of a 1200 yr proxy index for global volcanism, Earth Syst. Sci. Data, 5, 187–197, doi:10.5194/essd-5-187-2013, 2013.

Dameris, M., Matthes, S., Deckert, R., Grewe, V., and Ponater, M.: Solar cycle effect delays onset of ozone recovery, Geophys. Res. Lett., 33, L03806, doi:10.1029/2005GL024741, 2006.

de Laat, A. T. J. and van Weele, M.: The 2010 Antarctic ozone hole: observed reduction in ozone destruction by minor sudden stratospheric warmings, Sci. Rep., 1, 38, doi:10.1038/srep00038, 2011.

Dudok de Wit, T., Kretzschmar, M., Lilensten, J., and Woods, T.: Finding the best proxies for the solar UV irradiance, Geophys. Res. Lett., 36, L10107, doi:10.1029/2009GL037825, 2009.

Ebdon, R. A.: Notes on the wind flow at 50 mb in tropical and sub-tropical regions in January 1957 and January 1958, Q. J. Roy. Meteor. Soc., 86, 540–542, 1960.

Engel, A., Möbius, T., Bönisch, H., Schmidt, U., Heinz, R., Levin, I., Atlas, E., Aoki, S., Nakazawa, T., Sugawara, S., Moore, F., Hurst, D., Elkins, J., Schauffler, S., Andrews, A., and Boering, K.: Age of stratospheric air unchanged within uncertainties over the past 30 years, Nat. Geosci., 2, 28–31, doi:10.1038/ngeo388, 2009.

Eyring, V., Waugh, D. W., Bodeker, G. E., Cordero, E., Akiyoshi, H., Austin, J., Beagley, S. R., Boville, B. A., Braesicke, P., Brühl, C., Butchart, N., Chipperfield, M. P., Dameris, M., Deckert, R., Deushi, M., Frith, S. M., Garcia, R. R., Gettelman, A., Giorgetta, M. A., Kinnison, D. E., Mancini, E., Manzini, E., Marsh, D. R., Matthes, S., Nagashima, T., Newman, P. A., Nielsen,

J. E., Pawson, S., Pitari, G., Plummer, D. A., Rozanov, E., Schraner, M., Scinocca, J. F., Semeniuk, K., Shepherd, T. G., Shibata, K., Steil, B., Stolarski, R. S., Tian, W., and Yoshiki, M.: Multimodel projections of stratospheric ozone in the 21st century, J. Geophys. Res., 112, D16303, doi:10.1029/2006JD008332, 2007.

Fioletov, V. E. and Shepherd, T. G.: Seasonal persistence of midlatitude total ozone anomalies, Geophys. Res. Lett., 30, 1417, doi:10.1029/2002GL016739, 2003.

Graystone, P.: Meteorological office discussion on tropical meteorology, Meteorol. Mag., 88, 117, 1959.

Haigh, J. D. and Roscoe, H. K.: Solar influences on polar modes of variability, Meteorol. Z., 15, 371–378, 2006.

Ho, M., Kiem, A. S., and Verdon-Kidd, D. C.: The Southern Annular Mode: a comparison of indices, Hydrol. Earth Syst. Sci., 16, 967–982, doi:10.5194/hess-16-967-2012, 2012.

Huang, T. Y. W. and Massie, S. T.: Effect of volcanic particles on the O_2 and O_3 photolysis rates and their impact on ozone in the tropical stratosphere, J. Geophys. Res., 102, 1239–1249, doi:10.1029/96JD02967, 1997.

Jiang, X., Pawson, S., Camp, C. D., Nielsen, J. E., Shia, R.-L., Liao, T., Limpasuvan, V., and Yung, Y. L.: Interannual variability and trends of extratropical ozone. Part II: Southern Hemisphere, J. Atmos. Sci., 65, 3030–3041, doi:10.1175/2008JAS2793.1, 2008.

Kirtman, B., Power S., Adedoyin, A. J., Boer, G., Bojariu, R., Camilloni, I., Doblas-Reyes, F., Fiore, A., Kimoto, M., Meehl, G., Prather, M., Sarr, A., Schär, C., Sutton, R., van Oldenborgh, G.-J., Vecchi, G., and Wang, H.-J.: Near-term climate change: projections and predictability, in: Climate Change 2013: The Physical Science Basis. Contribution of Working Group I to the Fifth Assessment Report of the Intergovernmental Panel on Climate Change, edited by: Stocker et al., Cambridge University Press, Cambridge, UK and New York, NY, USA, in press, 2013.

Klekociuk, A. R., Tully, M. B., Alexander, S. P., Dargaville, R. J., Deschamps, L. L., Fraser, P. J., Gies, H. P., Henderson, S. I., Javorniczky, J., Krummel, P. B., Petelina, S. V., Shanklin, J. D., Siddaway, J. M., and Stone, K. A.: The Antarctic ozone during 2010, Austr. Meterol. Oceanogr. J., 61, 253–267, 2011.

Knibbe, J. S., van der A, R. J., and de Laat, A. T. J.: Spatial regression analysis on 32 years total column ozone data, Atmos. Chem. Phys. Discuss., 14, 5323–5373, doi:10.5194/acpd-14-5323-2014, 2014.

Kramarova, N. A., Nash, E. R., Newman, P. A., Bhartia, P. K., McPeters, R. D., Rault, D. F., Seftor, C. J., Xu, P. Q., and Labow, G. J.: Measuring the Antarctic ozone hole with the new Ozone Mapping and Profiler Suite (OMPS), Atmos. Chem. Phys., 14, 2353–2361, doi:10.5194/acp-14-2353-2014, 2014.

Kuttippurath, J., Goutail, F., Pommereau, J.-P., Lefèvre, F., Roscoe, H. K., Pazmiño, A., Feng, W., Chipperfield, M. P., and Godin-Beekmann, S.: Estimation of Antarctic ozone loss from ground-based total column measurements, Atmos. Chem. Phys., 10, 6569–6581, doi:10.5194/acp-10-6569-2010, 2010.

Kuttippurath, J., Lefèvre, F., Pommereau, J.-P., Roscoe, H. K., Goutail, F., Pazmiño, A., and Shanklin, J. D.: Antarctic ozone loss in 1979–2010: first sign of ozone recovery, Atmos. Chem. Phys., 13, 1625–1635, doi:10.5194/acp-13-1625-2013, 2013.

Labitzke, K.: On the signal of the 11-Year sunspot cycle in the Stratosphere over the Antarctic and its modulation by the Quasi-Biennial Oscillation (QBO), Meteorol. Z., 13, 263–270, 2004.

Naujokat, B.: An update of the observed quasi-biennial oscillation of the stratospheric winds over the tropics, J. Atmos. Sci., 43, 1873–1877, 1986.

Newman, P. A., Nash, E. R., Kawa, S. R., Montzka, S. A., and Schauffler, S. M.: When will the Antarctic ozone hole recover?, Geophys. Res. Lett., 33, L12814, doi:10.1029/2005GL025232, 2006.

Newman, P. A., Daniel, J. S., Waugh, D. W., and Nash, E. R.: A new formulation of equivalent effective stratospheric chlorine (EESC), Atmos. Chem. Phys., 7, 4537–4552, doi:10.5194/acp-7-4537-2007, 2007.

Poberaj, C. S., Staehelin, J., and Brunner, D.: Missing stratospheric ozone decrease at Southern Hemisphere middle latitudes after Mt. Pinatubo: a dynamical perspective, J. Atmos. Sci., 68, 1922–1945, doi:10.1175/JAS-D-10-05004.1, 2011.

Randel, W. J., Wu, F., and Stoarski, R.: Changes in column ozone correlated with the stratospheric EP flux, J. Meteorol. Soc. Jpn., 80, 849–862, 2002.

Roscoe, H. K. and Haigh, J. D.: Influences of ozone depletion, the solar cycle and the QBO on the Southern Annular Mode, Q. J. Roy. Meteor. Soc., 133, 1855–1864, 2007.

Rozanov, E. V., Schlesinger, M. E., Andronova, N. G., Yang, F., Malyshev, S. L., Zubov, V. A., Egorova, T. A., and Li, B.: Climate/chemistry effects of the Pinatubo volcanic eruption simulated by the UIUC stratosphere/troposphere GCM with interactive photochemistry, J. Geophys. Res., 107, 4594, doi:10.1029/2001JD000974, 2002.

Salby, M. L., Titova, E. A., and Deschamps, L.: Rebound of Antarctic ozone, Geophys. Res. Lett., 38, L09702, doi:10.1029/2011GL047266, 2011.

Salby, M., Titova, E., and Deschamps, L.: Changes of the Antarctic ozone hole: controlling mechanisms, seasonal predictability, and evolution, J. Geophys. Res., 117, D10111, doi:10.1029/2011JD016285, 2012.

Sato, M., Hansen, J. E., McCormick, M. P., and Pollack, J. B.: Stratospheric aerosol optical depths, 1850–1990, J. Geophys. Res., 98, 22987–22994, doi:10.1029/93JD02553, 1993.

Soukharev, B. E. and Hood, L. L.: Solar cycle variation of stratospheric ozone: multiple regression analysis of long-term satellite data sets and comparisons with models, J. Geophys. Res., 111, D20314, doi:10.1029/2006JD007107, 2006.

Stiller, G. P., von Clarmann, T., Höpfner, M., Glatthor, N., Grabowski, U., Kellmann, S., Kleinert, A., Linden, A., Milz, M., Reddmann, T., Steck, T., Fischer, H., Funke, B., López-Puertas, M., and Engel, A.: Global distribution of mean age of stratospheric air from MIPAS SF_6 measurements, Atmos. Chem. Phys., 8, 677–695, doi:10.5194/acp-8-677-2008, 2008.

Telford, P., Braesicke, P., Morgenstern, O., and Pyle, J.: Reassessment of causes of ozone column variability following the eruption of Mount Pinatubo using a nudged CCM, Atmos. Chem. Phys., 9, 4251–4260, doi:10.5194/acp-9-4251-2009, 2009.

The Montreal Protocol on Substances that Deplete the Ozone Layer: United Nations Environment Programme, Nairobi, Kenya, 2012.

Thompson, D. W. J. and Wallace, J. M.: Annular modes in the extratropical circulation, Part I: Month-to-month variability, J. Climate, 13, 1000–1016, 2000.

Tomé, A. R., and Miranda, P. M. A.: Piecewise linear fitting and trend changing points of climate parameters, Geophys. Res. Lett., 31, L02207, doi:10.1029/2003GL019100, 2004.

van der A, R. J., Allaart, M. A. F., and Eskes, H. J.: Multi sensor reanalysis of total ozone, Atmos. Chem. Phys., 10, 11277–11294, doi:10.5194/acp-10-11277-2010, 2010.

Vyushin, D., Fioletov, V. E., and Shepherd, T. G.: Impact of long-range correlations on trend detection in total ozone, J. Geophys. Res., 112, D14307, doi:10.1029/2006JD008168, 2007.

Weber, M., Dhomse, S., Wittrock, F., Richter, A., Sinnhuber, B.-M., and Burrows, J. P.: Dynamical control of NH and SH winter/spring total ozone from GOME observations in 1995–2002, Geophys. Res. Lett., 30, 1853, doi:10.1029/2002GL016799, 2003.

Weber, M., Dikty, S., Burrows, J. P., Garny, H., Dameris, M., Kubin, A., Abalichin, J., and Langematz, U.: The Brewer–Dobson circulation and total ozone from seasonal to decadal time scales, Atmos. Chem. Phys., 11, 11221–11235, doi:10.5194/acp-11-11221-2011, 2011.

World Meteorological Organization: Scientific Assessment of Ozone Depletion: 2006, Global Ozone Research and Monitoring Project – Report No. 50, Geneva, Switzerland, 572 pp., 2007.
World Meteorological Organization: Scientific Assessment of Ozone Depletion: 2010, Global Ozone Research and Monitoring Project – Report No. 52, Geneva, Switzerland, 516 pp., 2011.
Yang, E.-S., Cunnold, D. M., Newchurch, M. J., Salawitch, R. J., McCormick, M. P., Russell III, J. M., Zawodny, J. M., and Oltmans, S. J.: First stage of Antarctic ozone recovery, J. Geophys. Res., 113, D20308, doi:10.1029/2007JD009675, 2008.

Table 1. Summary of the uncertainties for the proxies discussed in Sects. 2.1 to 2.9 and their inclusion in the regression analysis in this study.

regressor	variations
Average EP flux	– 70 hPa, 40–90° S, Aug–Sep (baseline)
– 8 scenarios	– 70 hPa, 40–90° S, Jul–Aug
	– 70 hPa, 40–90° S, Jul–Sep
	– 70 hPa, 40–90° S, Jul
	– 70 hPa, 40–90° S, Aug
	– 70 hPa, 40–90° S, Sep
	– 70 hPa, 45–75° S, Aug–Sep
	– 100 hPa, 40–90° S, Aug–Sep
Solar flux–QBO index	– Random variations in Solar flux–QBO anomalies
– 100 Monte Carlo series	– 200 % Gaussian noise variations on single solar flux–QBO anomalies
SAM index	– 100 % random error on annual mean SAM index values
– 100 Monte Carlo series	
EESC loading	– EESC shapes based on different age of air of 2.5, 4.0 and 5.5 years
– 3 scenarios	
Volcanic aerosol	– Baseline Volcanic Aerosol index (NASA GISS)
– 6 scenarios	– Pinatubo peak comparable to El Chichón peak
	– Pinatubo peak twice the El Chichón peak
	– Pinatubo peak five times the El Chichón peak
	– El Chichón peak shifted one year back compared to Pinatubo
	– Pinatubo peak shifted one year back compared to El Chichón
Ozone record	– Sep-Oct-Nov average ozone (baseline)
– 8 scenarios	– Sep–Oct average ozone
	– Sep average ozone
	– Oct average ozone
	– 7 Sep–13 Oct average ozone
	– Very short 21–30 Sep average ozone
	– Very long 19 Jul–1 Dec average ozone
	– "Worst" 30 day average ozone.

Table 2. EESC-based Antarctic vortex core ozone trends and their 2σ trend uncertainties (DU/year) derived from multi-variate linear regression.

	Kuttippurath et al. (2013)		This study		
Period	EESC	PWLT	EESC	PWLT	LINT
1979–1999	−4.50 ± 0.65	−5.02 ± 1.11	−5.26 ± 0.21	−4.78 ± 1.10	−5.39 ± 1.24
2000–2010	1.11 ± 0.16	2.91 ± 2.73	1.02 ± 0.12	3.76 ± 9.88	1.19 ± 3.94
1979–1999			−5.26 ± 0.21	−4.86 ± 1.06	−5.43 ± 1.19
2000–2012			1.09 ± 0.10	3.42 ± 5.42	1.74 ± 3.06

Table 3. Cross correlations and their 2σ variance between explanatory variables.

	EPFLUX	EESC	AEROSOL	SF × QBO
SAM	−0.31 ± 0.27	−0.03 ± 0.17	−0.09 ± 0.19	−0.09 ± 0.29
SF × QBO	0.08 ± 0.28	0.07 ± 0.42	−0.02 ± 0.19	
AEROSOL	0.05 ± 0.17	0.03 ± 0.30		
EESC	0.25 ± 0.17			

Table 4. Fraction of statistically significant trends (%) in all regression results for different break years, period lengths and different types of trend calculations.

Start year	End year	Length	significant trends
2000	2010	11	0.9 %
1999	2010	12	4.5 %
1998	2010	13	14.1 %
2000	2012	13	1.5 %
1999	2012	14	9.0 %
1998	2012	15	21.5 %

Table 5. Percentage of statistically significant regressions for each combination of ozone and EP flux scenarios, as defined in Sect. 2, based on the PWLT regression model. Each ensemble consists of results of 180 000 single regressions (6 volcanic aerosol scenarios, 100 SAM and 100 QBO-solar index Monte Carlo runs, 3 break years).

EP flux / Ozone	Aug–Sep	Jul–Aug	Jul–Sep	Jul	Aug	Sep	45–75° S	100 hPa
Sep–Nov	13.2	2.3	11.3	0.2	1.6	12.0	14.3	19.6
Sep–Oct	24.6	7.2	23.9	1.1	1.1	40.3	18.9	28.7
Sep	0.6	0.6	1.6	0.1	0.2	2.0	0.3	0.7
Oct	45.4	10.4	32.1	2.0	2.8	51.9	43.0	49.1
21–30 Sep	< 0.1	< 0.1	< 0.1	< 0.1	< 0.1	< 0.1	< 0.1	< 0.1
7 Sep–13 Oct	0.6	0.2	0.7	0.1	< 0.1	1.9	0.4	1.1
Worst 30 days	3.4	1.6	3.9	0.4	0.2	10.3	1.5	3.1
19 Jul–1 Dec	10.4	3.2	10.1	0.4	1.9	11.2	10.2	14.8

Table 6. As Table 5 but for the break year 1997 and the period ending in 2012.

EP flux / Ozone	Aug–Sep	Jul–Aug	Jul–Sep	Jul	Aug	Sep	45–75° S	100 hPa
Sep–Nov	47.3	6.1	35.0	0.1	5.5	36.8	53.9	65.3
Sep–Oct	70.7	14.8	62.3	0.5	2.1	81.2	63.2	79.0
Sep	1.3	1.1	3.4	0.1	0.2	4.0	0.6	1.8
Oct	91.8	10.2	66.6	0.1	2.4	89.3	92.1	94.3
21–30 Sep	< 0.1	< 0.1	< 0.1	< 0.1	< 0.1	< 0.1	< 0.1	< 0.1
7 Sep–13 Oct	1.9	0.4	1.4	< 0.1	< 0.1	4.5	1.1	3.6
Worst 30 days	9.3	1.8	7.4	0.1	0.1	20.9	4.0	9.4
19 Jul–1 Dec	39.7	10.6	34.0	0.6	7.1	37.4	41.2	55.9

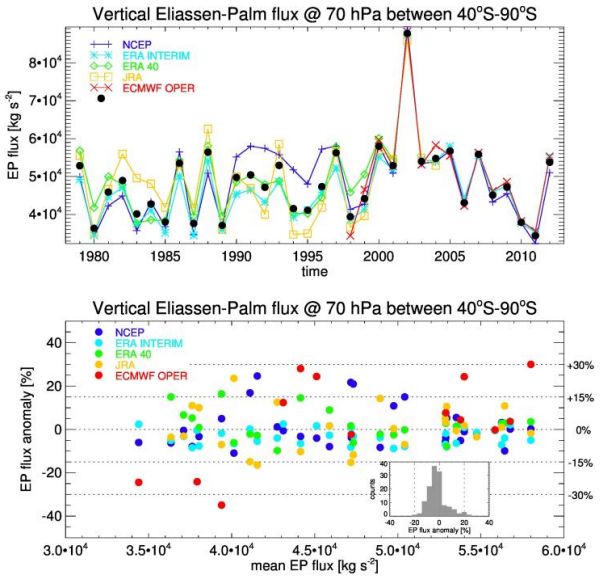

Figure 1. Vertical Eliassen–Palm (EP; $kg\,s^{-2}$) flux at 70 hPa between 40° S and 90° S for five different meteorological datasets for the period 1979–2012 averaged for the two month period August–September: NCEP reanalysis 1979–2012, ECMWF ERA INTERIM 1979–2012, ECMWF ERA 40 1979–2001, Japan Reanalysis 1979–2005, ECMWF operational analysis 1998–2012. Top panel shows the EP flux as function of time, including the mean EP flux for each year based on all datasets. Bottom panel shows the EP flux anomalies (%) of a given year as function of the mean EP flux (black dots in the upper panel) for all meteorological datasets available for that year. The insert shows the probability distribution of the relative anomalies. Data is obtained from the EP flux data website of the Alfred Wegener Institute (AWI) for Polar and Marine Research in Bremerhaven, Germany.

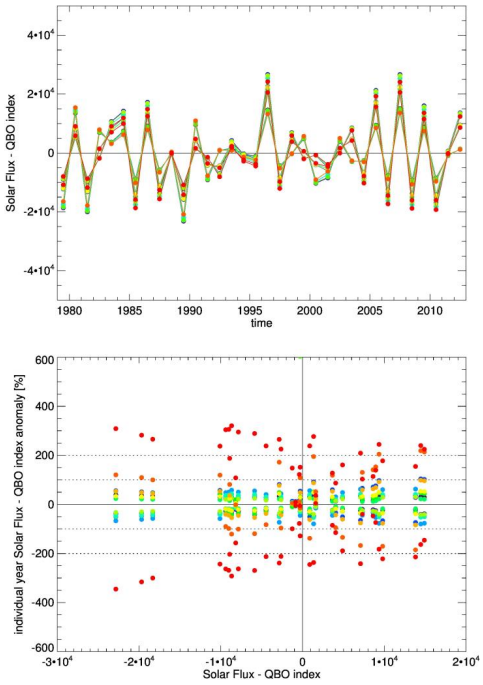

Figure 2. Time series of the combined Solar flux–QBO index (arbitrary units) (upper plot) and the index anomalies relative to the average of different possibilities to derive at the index. The Solar flux and QBO anomalies were calculated based both on the average as well as the range of Solar flux and QBO values (see Sect. 2.5 for the explanations of the "range"), and for both the entire record of Solar flux and QBO values (1947–2012 and 1953–2012, respectively) as well as for the period 1979–2012, resulting in a total of 16 combinations. The different colors denote the different combinations.

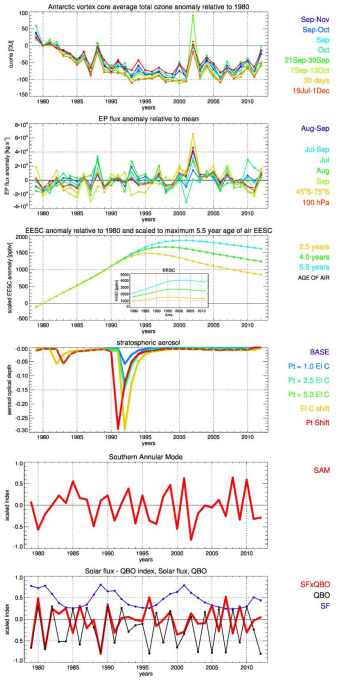

Figure 3. Time series of regressors for the period 1979–2012. For ozone, EP flux, EESC and stratospheric aerosol all scenarios as defined in Sect. 2 are included (indicated by the different colors). For the SAM and the solar flux–QBO index only the baseline time series is shown, and both indices – being unitless to start with – are scaled for proper comparison. Ozone values are in DU, EP fluxes are in $kg\,s^{-1}$, EESC values are in ppbv and stratospheric aerosol is in optical depth.

Discussion Paper | Discussion Paper | Discussion Paper | Discussion Paper |

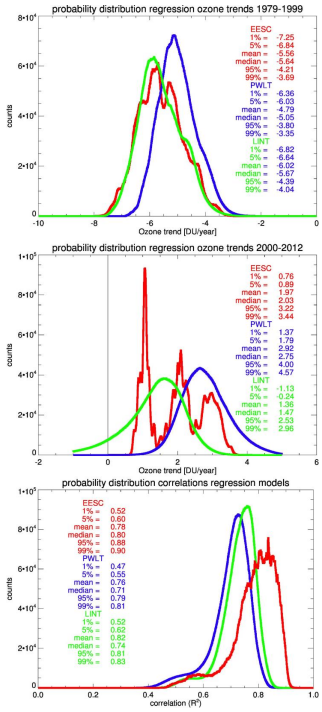

Figure 4. Probability distribution of ozone trends for the period 1979–1999 (upper plot) and 2000–2012 (middle plot) as well as time correlations (R^2) for the regression models and the ozone record scenarios (lower plot). The colors indicate the distributions for the three different long-term ozone regressions (EESC, PWLT and LINT). Indicated in the figure are also the 1–5 %-mean-media-95–99 % probability values of trends and correlations.

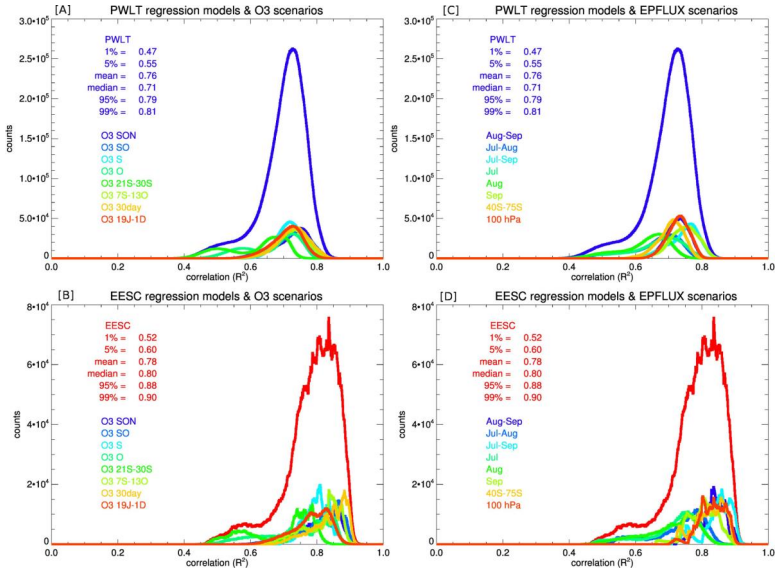

Figure 5. Probability distribution of regression model – ozone scenario correlations as Fig. 4, lower plot, for the PWLT and EESC regression model and sensitivity to the different ozone scenarios and different EP flux scenarios, indicated by the different colors.

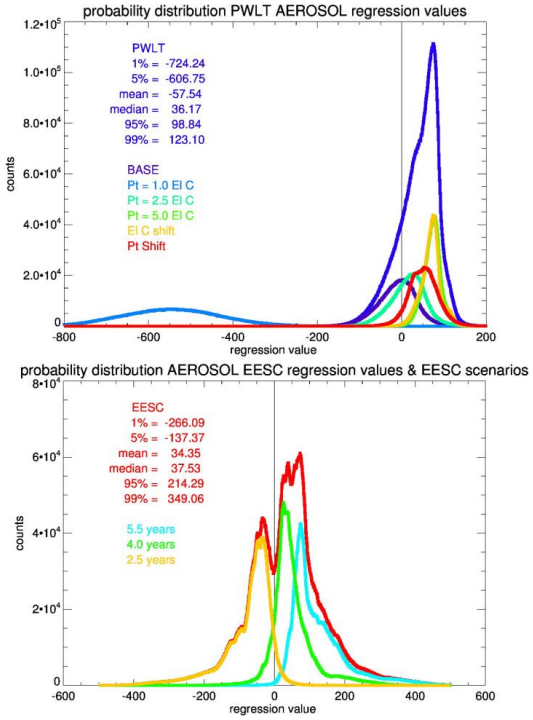

Figure 6. Upper panel: probability distribution of aerosol scenario regression coefficient values of all PWLT regression results. Included are also the distributions for the different stratospheric aerosol scenarios, indicated by the different colors. Lower panel: probability distribution of the EESC regression coefficient values of all EESC regression model results. Included are also the distributions for the three different EESC age of air scenarios, indicated by the different colors.

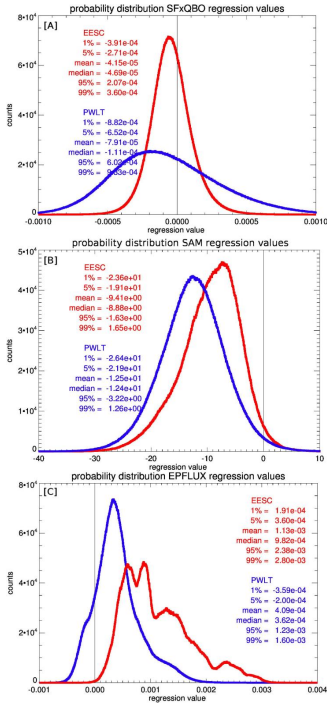

Figure 7. (A) Probability distribution of the solar flux–QBO index regression coefficient values of all EESC and PWLT regression model results. **(B)** Probability distribution of the SAM index regression coefficient values of all EESC and PWLT regression model results. **(C)** Probability distribution of the EP flux regression coefficient values of all EESC and PWLT regression model results.

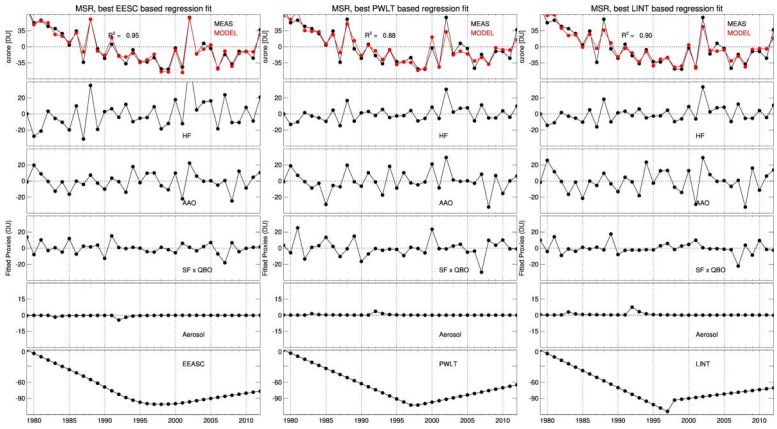

Figure 8. Optimal regression model result for the EESC, PWLT and LINT regressions (upper panels, red line) as well as the corresponding ozone record scenario (upper panel, black line). The ozone variations attributable to each are also shown. Ozone and ozone anomalies are given in DU.

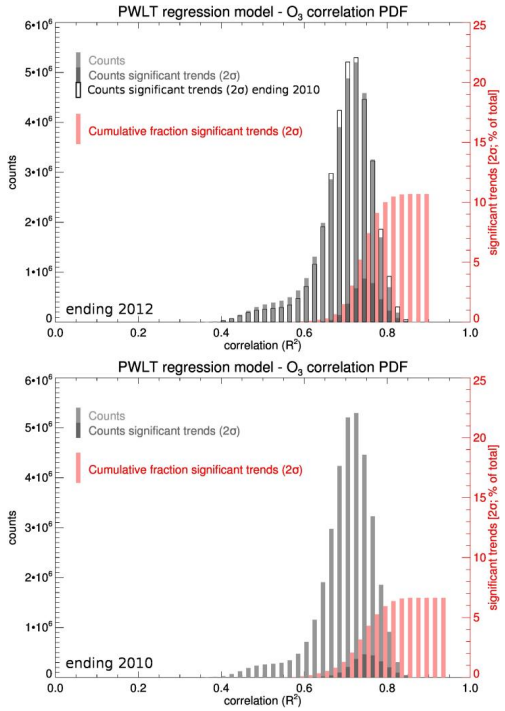

Figure 9. The probability distribution of regression model – ozone record scenario correlations (R^2) as shown in Fig. 5 for the PWLT regressions and the cumulative fraction of statistically significant (2σ) ozone trends for each correlation interval (red, right axis). The lower panel shows the distribution for the regressions ending in 2010, the upper panel for the regressions ending in 2012. Indicated in the upper panel is also the distribution of the regressions ending in 2010.